Enhanced Catalytic Performance for Propene Epoxidation with H_2 and O_2 over Bimetallic Au−Ag/Uncalcined Titanium Silicate-1 Catalysts

Xiang Feng,*[,†,‡] Jia Yang,[†] Xuezhi Duan,[†] Yueqiang Cao,[†] Bingxu Chen,[†] Wenyao Chen,[†] Dong Lin,[‡] Gang Qian,[†] De Chen,[§] Chaohe Yang,[‡] and Xinggui Zhou*[,†]

[†]State Key Laboratory of Chemical Engineering, East China University of Science and Technology, 130 Meilong Road, Shanghai 200237, China

[‡]State Key Laboratory of Heavy Oil Processing, China University of Petroleum, Qingdao 266580, China

[§]Department of Chemical Engineering, Norwegian University of Science and Technology, Trondheim 7491, Norway

Supporting Information

ABSTRACT: Gradually emerging environmental concerns have triggered the development of highly efficient catalysts for propene epoxidation with H_2 and O_2. Unfortunately, intensifying the activity and stability is still a challenging task. Herein, Au−Ag bimetallic catalysts were deposited on titanium silicate-1 with blocked pores (TS-1-B). Via density functional theory calculations together with multiple types of characterization (e.g., high-angle annular dark-field scanning transmission electron microscopy, ultraviolet−visible, and X-ray photoelectron spectrometry), we found that the synergy between Au and Ag significantly improved the catalytic performance via not only the decrease in the Au nanoparticle size but also the enhanced oxygen adsorption and electron transfer ability from Au to O_2. Furthermore, a volcano-shaped relationship between the Au/Ag ratio and catalytic performance was also established, and the Au_{10}−Ag_1/TS-1-B catalyst showed an excellent stable PO formation rate (174−233 g_{PO} h^{-1} g_{Au}^{-1}) and a H_2 efficiency of 44%, higher than those of the reported stable catalysts. The insights and methodology reported here may pave the way for maximizing Au utilization efficiency and unraveling the intrinsic structure−performance relationship of bimetallic catalysts for propene epoxidation.

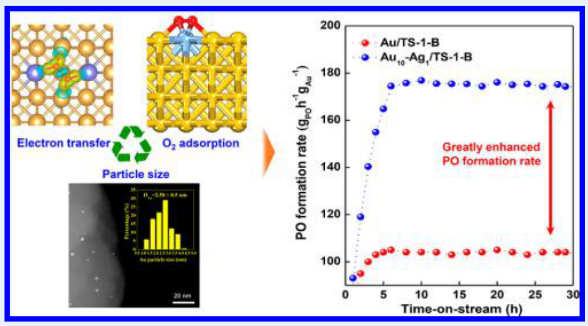

KEYWORDS: *propene epoxidation, Au−Ag bimetallic catalysts, TS-1-B, DFT, synergy*

1. INTRODUCTION

Propylene oxide (PO) harbors tremendous potential as an important bulk chemical intermediate in petrochemical industries for the production of polyurethane and polyester resins. Utilization of propylene, H_2, and O_2 to produce PO provides a greener, simpler, and more sustainable route and can liberate us from the reliance on traditional chlorohydrin and several organic hydroperoxide processes. In 1998, Haruta[1] first reported that gold nanoparticles deposited on Ti-containing supports are active for the reaction. Subsequently, most studies have focused on the rational design and optimization of Au-based/Ti-containing support catalysts to improve the catalytic performance toward practical applications.[2−6] It is widely accepted that highly dispersed Au nanoparticles and isolated Ti (IV) sites are indispensable for PO formation, and the Au/titanium silicate-1 (TS-1) catalyst shows a superior PO formation rate.[7] Meanwhile, the reaction pathways first proceed by the reaction between H_2 and O_2 on Au nanoparticles to form hydrogen peroxide (H_2O_2). The H_2O_2 subsequently diffuses to the nearby isolated tetrahedral Ti^{4+} sites to generate Ti-OOH species that epoxidize propene to PO.[4,8,9]

When the remarkable structural sensitivity of propene epoxidation with H_2 and O_2 and the high cost of the Au catalyst are taken into account, understanding the nature and maximizing the utilization efficiency of Au nanoparticles are of prime scientific and industrial importance.[2,5,10−14] In our previous works,[15−17] both experimental and theoretical analyses demonstrate that smaller Au nanoparticles have more active sites and thus give rise to a much higher PO formation rate. Considering that Au nanoparticles with a much smaller particle size are not easily prepared by the widely used deposition−precipitation method,[18,19] it is highly desirable to obtain smaller Au nanoparticles by modified deposition−

Received: April 4, 2018
Revised: June 7, 2018
Published: July 13, 2018

precipitation methods or adding the second metal as a promoter.[11,20−22] Lu et al.[23] proposed that alkali metals (e.g., K and Cs) and alkaline earth metals (e.g., Mg, Ca, Sr, and Ba) could increase the capturing efficiency and dispersion of Au and hence increase the catalytic activity. It is reported that the Cs promoter enables more tiny Au clusters to be located inside the TS-1 microporous channels (~0.5 nm).[20] The tiny Au clusters are more active toward PO formation and thus result in significantly increased activity. However, these Au clusters could lead to fast deactivation because of a severe micropore blocking phenomenon.[24] Therefore, designing a highly active Au-based catalyst with good stability is still challenging.

It is demonstrated that micropore blocking by carbonaceous deposits is the main deactivation mechanism for titanium silicate-1-supported Au catalysts (Au/TS-1),[12] leading to the invalidation of the Au particles inside TS-1 micropores. We therefore employed uncalcined TS-1 with blocked micropores (TS-1-B) to immobilize Au nanoparticles on the external surfaces of TS-1-B and thus to improve the stability of the catalysts for 30 h. To date, little attention has been focused on improving the catalytic performance of Au/TS-1-B catalysts. Therefore, there is an urgent need to develop a strategy to enhance the stable catalytic activity of Au/TS-1-B catalysts and also to elucidate the structure−performance relationship for the Au/Ti-based catalysts.

In this work, novel Au−Ag/TS-1-B bimetallic catalysts are prepared by a sequential deposition−precipitation method, and the underlying structure−performance relationship for direct propene epoxidation with H_2 and O_2 is systematically elucidated by multiple types of characterization [e.g., high-angle annular dark-field scanning transmission electron microscopy (HAADF-STEM), ultraviolet−visible (UV−vis), X-ray photoelectron spectrometry (XPS), powder X-ray diffraction (XRD), N_2 physisorption, and inductively coupled plasma atomic emission spectrometry (ICP-AES)] and density functional theory (DFT) calculation. It is found that the Ag/TS-1-B catalyst prepared by the deposition−precipitation method is almost inactive, while the introduction of Ag enhances the PO formation rate of the Au-based/TS-1-B catalyst. On one hand, the novel Au−Ag catalyst has a smaller nanoparticle size (~2.7 nm) and thus more active sites in comparison to the Au catalyst. On the other hand, the Au−Ag catalyst shows better oxygen adsorption and electron transfer ability, promoting electron transfer from Au to O_2. Moreover, a volcano-shaped relationship is observed between the PO formation rate and Au/Ag molar ratio. The Au−Ag/TS-1-B catalyst with a Au/Ag molar ratio of 10/1 shows an excellent stable PO formation rate (174−233 $g_{PO}\ h^{-1}\ g_{Au}^{-1}$), and the plausible Au/Ag ratio and activity relationship is further provided. The insights revealed herein could guide the rational design of Au-based/TS-1-B catalysts for propene epoxidation with H_2 and O_2. The methodology combining DFT, characterization, and experimental methods could also be helpful for elucidating the intrinsic properties of other bimetallic catalysts.

2. EXPERIMENTAL SECTION

2.1. Catalyst Preparation. *2.1.1. Preparation of TS-1 with Blocked Micropores.* TS-1 was synthesized using the hydrothermal method.[13,19] In a typical synthesis, 2.0 g of polyoxyethylene 20-sorbitan monolaurate (Tween 20, Aldrich) was added to 28.6 g of deionized water under vigorous stirring, followed by addition of 22.6 g of tetrapropylammonium hydroxide (TPAOH, 25 wt %) together with 40.53 g of tetraethylorthosilicate (TEOS, 95 wt %). After the mixture had been stirred for 1 h, 1.78 mL of titanium(IV) tetrabutoxide (TBOT, 99 wt %) mixed with 20 mL of isopropanol (IPA, 99.5 wt %) was added in a dropwise manner. This solution was placed in a Teflon autoclave and crystallized at 453 K for 48 h. Afterward, the as-synthesized TS-1 was washed thoroughly and dried under vacuum at room temperature. The TS-1 with blocked micropores by the remaining TPA^+ template is denoted as TS-1-B.

2.1.2. Preparation of Monometallic Catalysts. The Au/TS-1-B catalyst with a theoretical Au loading of 0.1 wt % was performed by a deposition−precipitation method with urea (DPU) in the absence of light according to the previous report[14] because the DPU method is easier and the reproducibility is better. Small amount of Na^+ is added during preparation. Typically, 0.5 g of TS-1-B, 0.05 mL of $HAuCl_4$ (4.85×10^{-2} M), and 0.045 g of urea were dissolved in 25 mL of deionized water. The slurry was stirred for 6 h at 363 K, centrifuged, washed, and then dried under vacuum at room temperature.

The Ag/TS-1-B catalyst was prepared by a deposition−precipitation method with NaOH as the precipitant (DP-NaOH).[25] Then 0.55 mL of $AgNO_3$ (8.4×10^{-4} M) and 0.5 g of TS-1 were dissolved in 25 mL of deionized water. The pH was adjusted to 9.0 by dropwise addition of NaOH (0.1 M). The solution was aged for 2 h at 353 K in the absence of light. The sample slurry was centrifuged, washed with water twice, and dried under vacuum at 303 K for 8 h.

2.1.3. Preparation of Bimetallic Catalysts. Au−Ag/TS-1-B catalysts were prepared by a sequential deposition−precipitation method, in which Ag was first deposited on TS-1-B by the DP-NaOH method. The loading of Ag was adjusted by changing the $AgNO_3$ concentration. Subsequently, Au was deposited by the DPU method. The theoretical Au loading is always kept at ~0.08 wt % for all samples, while the loading of Ag was tuned to synthesize Au−Ag catalysts with different Au/Ag atomic ratios of 30/1, 20/1, 10/1, 6/1, 2/1, and 1/1. The actual Au and Ag loadings of the bimetallic catalysts were also determined by ICP-AES, and the results are listed in Table S1. The Au−Ag bimetallic catalysts were denoted as Au_x−Ag_1/TS-1-B, where x stands for the actual Ag/Au molar ratio. For example, Au_{10}−Ag_1/TS-1-B represents a Au/Ag molar ratio of 10.

2.2. Catalytic Testing. The catalysts were tested for direct propene epoxidation with H_2 and O_2 in a quartz tubular reactor (inside diameter of 8 mm) under atmospheric pressure. Then 0.15 g of catalysts was sieved to 100 mesh size and reduced *in situ* in the reactor, which was heated from room temperature to 473 K at a rate of 1 K/min in a H_2/N_2 mixture (3/5 by volume) with a total flow rate of 40 mL/min. At 473 K, the reaction rates were measured in a reactant mixture of oxygen (99.999%), hydrogen (99.999%), propene (99.9%), and nitrogen (99.999%) with flow rates of 3.5, 3.5, 3.5, and 24.5 mL min^{-1}, respectively, and a space velocity of 14000 mL $h^{-1}\ g_{cat}^{-1}$. The reactants and products were analyzed by two online gas chromatographs (Agilent 6890), equipped with TCD (5A column and Porapak Q column) and FID (Porapak T column), respectively. The 5A (3 mm × 3 m) and Porapak Q (3 mm × 3 m) columns were used to detect hydrocarbons, H_2, O_2, N_2, CO_x, and H_2O, while the Porapak T column (3 mm × 3 m) was used to detect oxygenates (e.g., PO, propanal,

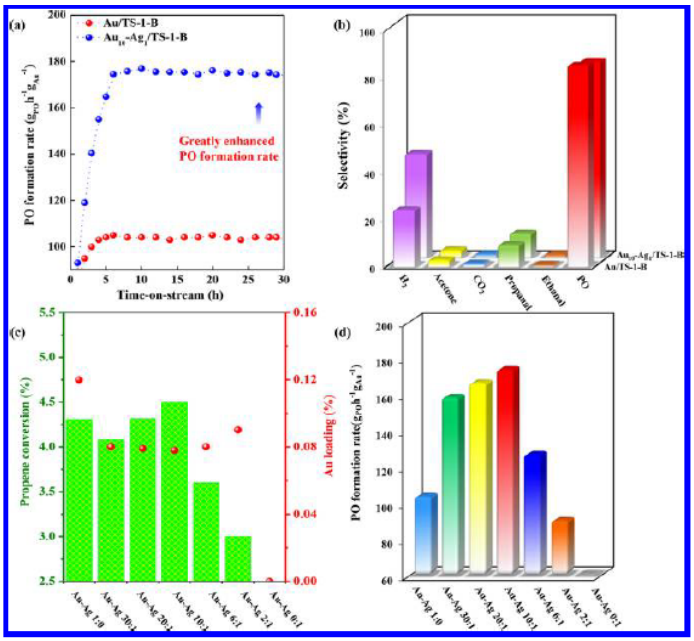

Figure 1. PO formation rate as a function of (a) time on stream and (b) selectivity of Au/TS-1-B and Au_{10}−Ag_1/TS-1-B catalysts. Propene conversions, (c) Au loadings, and (d) PO formation rates of Au/TS-1-B, Ag/TS-1-B, and Au−Ag/TS-1-B catalysts with different Au/Ag molar ratios.

and acetaldehyde), propene, and propane. The carbon balance, conversion, and selectivity were defined as follows:

$$\text{carbon balance} = [3 \times (\text{propene} + \text{PO} + \text{propanal} + \text{acetone}) + 2 \times \text{ethanal} + \text{CO}_2] / (3 \times \text{propene})$$

$$\text{propene conversion} = \text{moles of } (\text{C}_3\text{-oxygenates} + 2/3\text{ethanal} + \text{CO}_2/3)/\text{moles of propylene in the feed}$$

$$\text{C}_3\text{-oxygenate selectivity} = \text{moles of C}_3\text{-oxygenate}/\text{moles of } (\text{C}_3\text{-oxygenates} + 2/3\text{ethanal} + \text{CO}_2/3)$$

$$\text{ethanal selectivity} = 2/3(\text{mole of ethanal})/\text{moles of } (\text{C}_3\text{-oxygenates} + 2/3\text{ethanal} + \text{CO}_2/3)$$

$$\text{CO}_2 \text{ selectivity} = \text{moles of CO}_2/\text{moles of } (\text{C}_3\text{-oxygenates} + 2/3\text{ethanal} + \text{CO}_2/3)$$

$$\text{H}_2 \text{ efficiency} = \text{moles of PO/moles of H}_2 \text{ converted}$$

It should be noted that the CO_2 can be well-analyzed in this work, and the carbon balance is >95%.

2.3. Catalyst Characterizations. The loadings of Au and Ag on the catalysts were analyzed by ICP-AES with an Agilent 725-ES instrument. The crystal structures of catalysts were identified by XRD measurements (Cu Kα radiation, k = 0.15418 nm, 40 kV, 120 mA) using a Bruker D8 Advance instrument. HAADF-STEM images were obtained on a Tecnai G2 F20 S-Twin instrument equipped with a digitally processed STEM imaging system. Transmission electron microscopy (TEM) images were obtained on a JEOL JSM-2100F instrument with an accelerating voltage of 200 kV and a point resolution of 0.18 nm. The Cl contents of the catalysts were detected by ion chromatography on a Thermo Fisher ICS 1100 instrument. UV−vis diffuse reflectance spectra (UV−vis DRS) of the catalysts were obtained on a PerkinElmer Lambda 35 instrument. XPS was performed using a Kratos XSAM 800 spectrometer equipped with an Al Kα X-ray (1486.6 eV). The excitation source works at 15 kV, and the internal standard of the C 1s peak is set as 284.6 eV.

2.4. DFT Calculations. The DFT calculations were performed by employing the Vienna ab initio simulation package (VASP). The interaction between the valence electrons and the core was described by projected augmented wave potentials. The exchange correlation energy was calculated with generalized gradient approximation (GGA) based on the Perdew−Burke−Ernzerhof (PBE) functional. The Kohn−Sham orbitals were expanded in a plane wave basis set with a kinetic cutoff energy of 400 eV. On the basis of the lattice size, Monkhorst−Pack meshes of 5 × 5 × 1 k-point samplings in the surface Brillouin zones were used for the surfaces, 15 × 15 × 15 for the bulk Au, and 5 × 5 × 5 for the bulk Au−Ag. The geometry optimization was converged until the forces on each atom were <0.05 eV/Å and the total energy differences were $<10^{-7}$ eV. Two low-index facets, i.e., (100) and (111), were employed to calculate the adsorption energy of oxygen. The bulk of Au−Ag bimetal was modeled with 29 Au atoms and three Ag atoms. The surface slabs of Au and Au−Ag were modeled with p(3 × 3) and p(1 × 1) supercells,

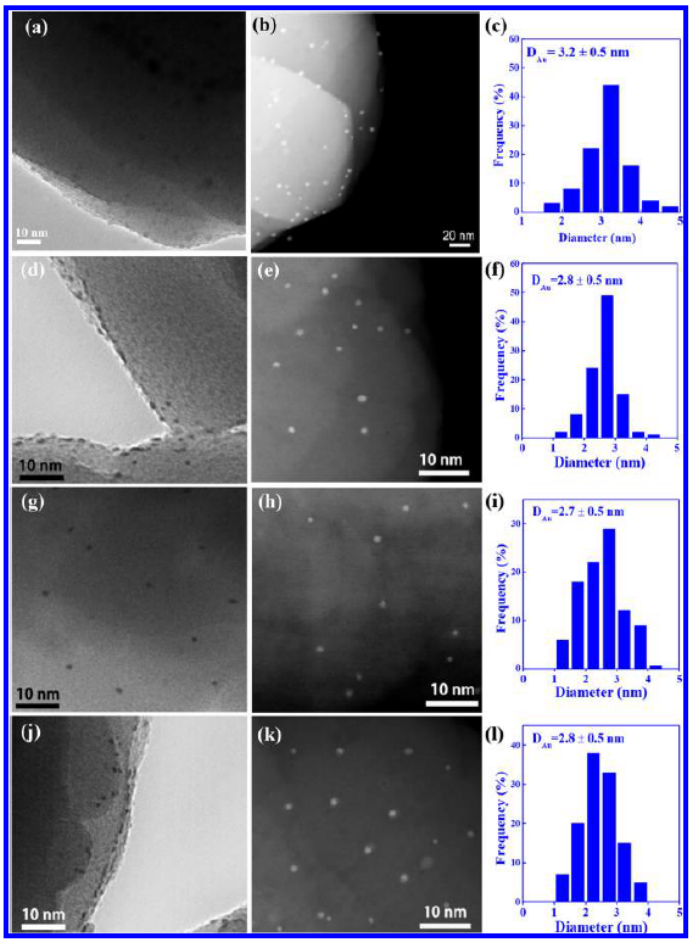

Figure 2. Representative HRTEM and HAADF-STEM images and particle size distributions of (a–c) Au/TS-1-B, (d–f) Au_{20}–Ag_1/TS-1-B, (g–i) Au_{10}–Ag_1/TS-1-B, and (j–l) Au_2–Ag_1/TS-1-B catalysts.

respectively, with four layers after optimizing the bulk. A 15 Å vacuum layer along the direction of the surface normal was used to avoid periodic interactions. The bottom two layers were fixed, and the top two layers as well as the adsorbate, i.e., O_2, were relaxed during geometry optimization. The adsorption energy of O_2 was calculated by the following equation:

$$E_{ads} = E_{O_2/surface} - E_{O_2} - E_{surface}$$

where $E_{O_2/surface}$ is the total energy of the surface adsorbed with the O_2, $E_{surface}$ is the total energy of the clean surface, and E_{O_2} is the total energy of isolated O_2.

The atomic charges of Au, Ag, and O were obtained by Bader analysis, which was implemented with a fast algorithm. The core charge density was included in the partitioning.[26,27] The charge density difference images of the O_2 adsorption were obtained by VESTA visualization software and calculated as $\Delta\rho(r) = \rho_{total}(r) - \rho_{surface}(r) - \rho_{oxygen}(r)$, where $\rho_{total}(r)$ is the electron density of the whole adsorbed system and $\rho_{surface}(r)$ and $\rho_{oxygen}(r)$ are the electron densities of the surface and the oxygen, respectively.

3. RESULTS AND DISCUSSION

3.1. Enhanced Catalytic Performance for Au–Ag/TS-1-B Catalysts. Au/TS-1-B, Ag/TS-1-B, and Au–Ag/TS-1-B catalysts were prepared by a deposition–precipitation method and tested for direct propene epoxidation with H_2 and O_2. Figure 1a shows the PO formation rate as a function of time on stream. Under the testing conditions, the Ag/TS-1-B catalyst is almost inactive for PO formation. This is possibly because H_2 and O_2 may not easily react with each other to form H_2O_2 for the subsequent epoxidation step[28,29] on Ag sites. In contrast, the introduction of a small amount of Ag greatly enhances the PO formation rate of the Au/TS-1-B catalyst from 104 to 174 $g_{PO}\ h^{-1}\ g_{Au}^{-1}$ at 200 °C. This clearly shows the promotional effect of Ag. The induction period for both Au/TS-1-B and Au–Ag/TS-1-B catalysts could be due to the decomposition of the template on the external surface and the release of active

sites.[9,24] In addition, Figure 1b shows the product selectivities of the two catalysts. The Au/TS-1-B catalyst has a PO selectivity of 85%, which is slightly higher than that of the Au_{10}–Ag_1/TS-1-B catalyst (i.e., 83%). Moreover, the stability tests with both Au/TS-1-B and Au_{10}–Ag_1/TS-1-B catalysts show that they both have good stability. This is because the presence of the TS-1-B support makes Au nanoparticles on the external surfaces of the support, suppressing the deactivation of micropore blocking.[12] Moreover, the hydrogen efficiency is also illustrated in Figure 1b. For the Au/TS-1-B catalyst, the hydrogen efficiency is ~22%, which is quite similar to that of the traditional 0.10 wt % Au/TS-1 catalyst. In comparison, the Au–Ag/TS-1-B catalyst has a higher efficiency of 44%. This indicates that H_2O_2 formed from hydrogen is efficiently used for the synthesis of PO rather than decomposition to H_2O.

The physicochemical properties of Au/TS-1-B and Au_{10}–Ag_1/TS-1-B catalysts are then analyzed to elucidate the intrinsic reason for the distinct catalytic performance. HRTEM and HAADF-STEM are first employed to characterize the size distribution of metal nanoparticles on Au/TS-1-B and Au_{10}–Ag_1/TS-1-B catalysts. As shown in Figure 2 (a–c and g–i), the two catalysts exhibit uniform and well-dispersed metal nanoparticles. More interestingly, the Au_{10}–Ag_1/TS-1-B catalyst (i.e., ~2.7 nm) has an average metal particle size that is smaller than that of the Au/TS-1-B catalyst (i.e., ~3.2 nm), suggesting the introduction of Ag favors the dispersion of Au on the TS-1-B surface. This could be mainly because Ag atoms with good mobility could easily move to Au particles and form the Au–Ag bimetallic nanoparticles, inhibiting Au agglomeration induced by Cl^- during the catalytic reduction process.[30–32] It is reported that the smaller Au nanoparticles are more active toward PO formation because of the presence of more active Au corner sites.[2,5,18,33–37] Therefore, the smaller nanoparticle size of Au_{10}–Ag_1/TS-1-B could be one reason for the enhanced PO formation rate. In addition, it could also be the reason for the higher hydrogen efficiency because a smaller Au size is favorable for H_2 utilization.[15]

The PO formation rate of the Au/TS-1-B catalyst follows the Au size dependence of $d^{-2.7}$ as reported in the literature.[15] Therefore, on the basis of the Au–Ag nanoparticle size (2.7 nm), the PO formation rate should be ~164 $g_{PO}\ h^{-1}\ g_{Au}^{-1}$, which is smaller than the experimental data (Figure 3). This indicates that the other effect also exists. The structures of Au–Ag and Au catalysts are then studied by XRD (Figure 4). Au/TS-1-B and Au–Ag/TS-1-B catalysts all exhibit a typical

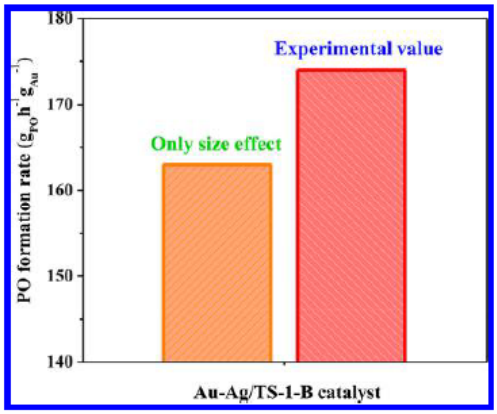

Figure 3. Experimental and calculated PO formation rates considering only the effect of size.

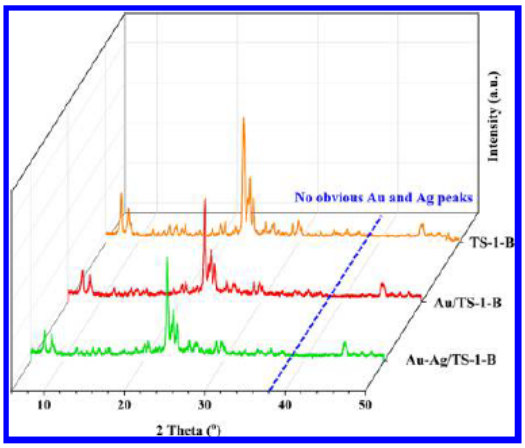

Figure 4. XRD patterns of the TS-1 support and Au/TS-1-B and Au_{10}–Ag_1/TS-1-B catalysts.

structure of MFI with high crystallinity. The single diffraction peak at ~24.5° is the evidence of the orthorhombic symmetry of the TS-1-B support.[16] It is also reported that both Au and Ag crystalline peaks are located at ~38.1° due to the same fcc structure and similar lattice constants (0.409 vs 0.408).[38,39] However, no obvious peaks ascribed to Au and Ag nanoparticles can be observed via XRD, indicating that metal nanoparticles are very small and well dispersed on the TS-1-B surface. This is in accordance with the HAADF-STEM and HRTEM characterizations (Figure 2a–l).

UV–vis spectroscopy is a powerful tool for investigating the structure of Au–Ag nanoparticles and thus is employed to probe the interaction between Au and Ag. There is only one legible adsorption band centered at ~220 nm on the UV–vis spectrum of the pure TS-1-B support (Figure S1), which is the characteristic peak of isolated tetrahedral Ti species. No anatase peak exists at 330 nm. This could guarantee the clear observation of Au, Ag, and Au–Ag absorption bands without interference of support adsorption bands. Figure 5 shows the UV–vis spectra of Au/TS-1-B, Ag/TS-1-B, and Au_{10}–Ag_1/TS-1-B catalysts and the physical mixture of Au/TS-1-B and Ag/TS-1-B. It is clear that Au/TS-1-B and Ag/TS-1-B present absorption bands at ~530 and ~400 nm, respectively. The physical mixture of Au/TS-1-B and Ag/TS-1-B shows both respective adsorption bands. In contrast, for the Au_{10}–Ag_1/TS-1-B catalyst, the characteristic adsorption band of Ag disappears, and the characteristic adsorption band of Au appears to be blue-shifted from 530 to 507 nm. Moreover, previous experimental and theoretical studies demonstrated that a Au–Ag alloy is the most likely form between Au and Ag, which could show only one peak in its UV–vis spectrum.[40–45] The results presented above indicate that the bimetallic nanoparticles most likely exist in the form of a Au–Ag alloy.

Besides the enhanced dispersion of Au nanoparticles (i.e., the geometric effects), introduction of Ag in principle could also affect the electronic property of Au. It is reported that O_2 could mainly adsorb on Au sites[4] or Au–Ti perimeters.[46] To better study the effect of the addition of Ag on the properties of Au and also to simplify the calculation, we first study the O_2

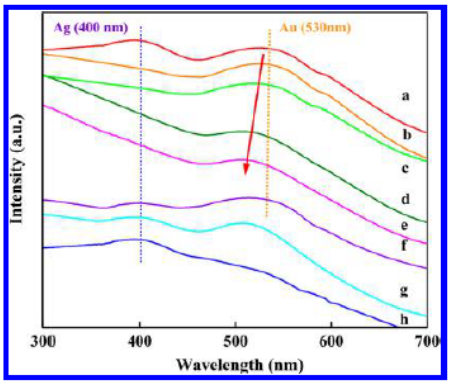

Figure 5. UV−vis DRS spectra of (a) the physical mixture of Au/TS-1-B and Ag/TS-1-B catalysts, (b) Au/TS-1-B, and Au−Ag/TS-1-B catalysts with different Au/Ag molar ratios: (c) Au_{30}−Ag_1, (d) Au_{20}−Ag_1, (e) Au_{10}−Ag_1, (f) Au_6−Ag_1, (g) Au_2−Ag_1, and (h) Ag/TS-1-B catalysts.

adsorption ability and electron transfer on Au and Au−Ag bimetallic nanoparticles by DFT calculations. Moreover, propene is not studied herein because propene is widely accepted to be better adsorbed on Ti^{4+} species from the mechanism.[4] Low-index (111) and (100) facets of Au and Au−Ag are used because they are relatively stable and easily exposed during reaction.[15,47] In our previous reports,[9,15] we also observed the representative Au shape of a truncated octahedron with top facets of (111) and (100). The adsorption of O_2 on Au and Au−Ag nanoparticles is investigated, and the results are shown in Figure 6. On the Au (111) surface, we consider O_2 adsorption at four different sites (top, fcc, hcp, and bridge). The detailed configurations and adsorption energy at each site are shown in Figure S2. It is found that the O_2 adsorption at the bridge site is much more favorable (E_{ads} = 0.51 eV) than at the top, fcc, and hcp sites for Au (111). As for Au (111), we also calculate the O_2 adsorption energy on Au (100), Au−Ag (111), and Au−Ag (100) at different sites (Figures S3−S5), and the stable configurations are shown in Figure 6. It is clear from Figure 6 that O_2 adsorption is stronger on the surfaces of Au−Ag bimetallic nanoparticles than on pure Au nanoparticles.

Moreover, the surface electronic properties are also studied to further understand the electronic modification of the Au−Ag/TS-1-B catalyst as well as the interaction between O_2 and the metals (Au and Au−Ag). The Bader charge calculations for Au atoms in pure Au surfaces and bimetallic Au−Ag surfaces are first performed, as shown in Figure S6. After the introduction of Ag atoms, the Au atoms on the surfaces of Au−Ag (111) and Au−Ag (100) are negatively charged with −0.08e and −0.13e, respectively. This negatively charged Au sites in bimetallic Au−Ag surfaces indicate that there is electron transfer from Ag to Au, which is also demonstrated by the decrease in the Au XPS binding energy[48] from 83.7 to <83.2 eV. When O_2 is adsorbed on Au and Au−Ag bimetallic catalysts, electron transfer is also investigated by Bader charge analysis. The charge density difference plots (Figure 7) clearly show the increase in the electron density of the oxygen when it was adsorbed on Au or Au−Ag surfaces. It is worth mentioning that the adsorbed oxygen withdraws more electron from the Au−Ag surface than from pure Au surfaces (Figure 8), suggesting the Ag-promoted Au surfaces tend to devote more electrons to the adsorbed oxygen and thus to activate it. These results show that a Au−Ag bimetallic structure could help to increase the tendency to lose electrons from Au nanoparticles, in accordance with the reaction mechanism of propene epoxidation[29] in which O_2 should accept the electron from Au nanoparticles, generating O_2^- for subsequent reaction. Therefore, the improved O_2 adsorption together with the better electron transfer ability of Au−Ag bimetallic nanoparticles to O_2 could be the other reason for enhanced catalytic performance.

XPS is also used to analyze the oxygen species on the surface of catalysts. Figure 9 shows the O_{1s} regions of Au/TS-1-B and Au_{10}−Ag_1/TS-1-B catalysts. It indicates the presence of three different oxygen species: (1) a mixture of hydroxyl groups and adsorbed water on the surface of the catalyst at ∼531.8 eV,[49] (2) oxygen atoms bonded to silicon lattice oxygen at ∼533.0 eV,[50] and (3) surface-active oxygen species (O_2^-) at ∼532.5 eV.[51] The percentage of O_2^- oxygen species adsorbed on the surface of the Au_{10}−Ag_1/TS-1-B catalyst is 12.9%, higher than

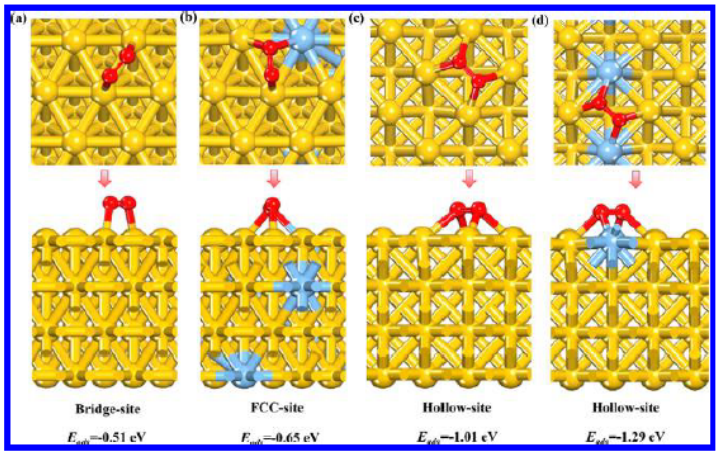

Figure 6. Stable O_2 adsorption configurations and adsorption energy for (a) Au (111), (b) Au−Ag (111), (c) Au (100), and (d) Au−Ag (100).

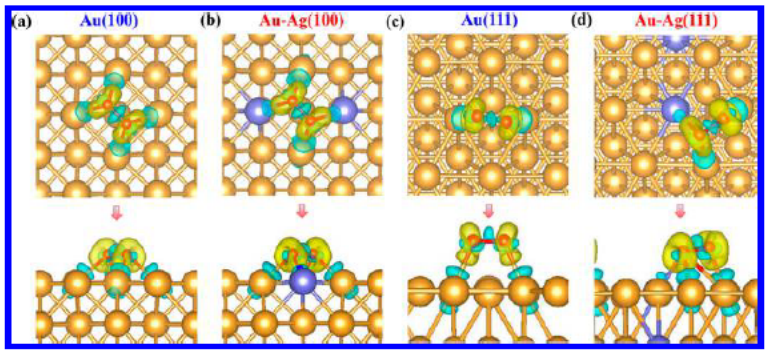

Figure 7. Charge density difference of O_2 adsorbed on Au (100), Au−Ag (100), Au (111), and Au−Ag (111) surfaces. Yellow and light blue isosurfaces denote increases and decreases of 0.005 e/Å^3, respectively.

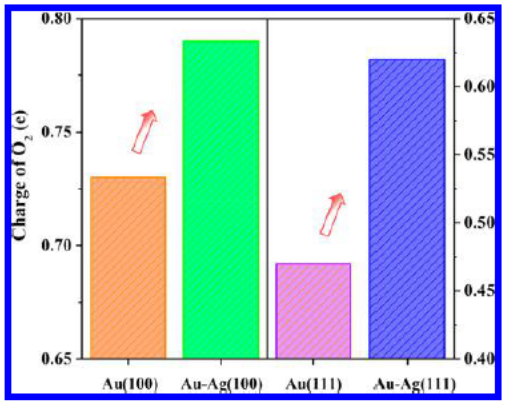

Figure 8. Absolute values of the net charge of the O_2 in the adsorbed states on Au (100), Au−Ag (100), Au (111), and Au−Ag (111) surfaces.

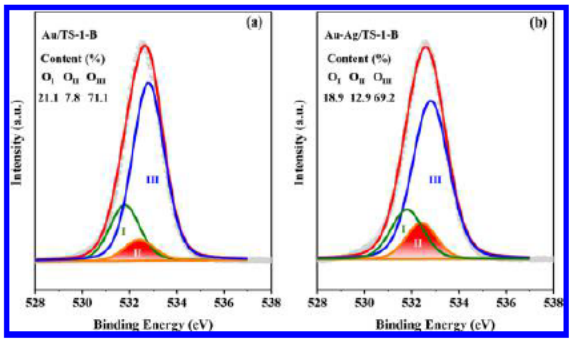

Figure 9. XPS peaks of O_{1s} regions on (a) Au/TS-1-B and (b) Au_{10}−Ag_1/TS-1-B catalysts.

that of 7.8% on the Au/TS-1-B catalyst. The unique structure of Au−Ag nanoparticles could accelarate the electron transfer to the antibonding orbital of the O_2 molecule and facilitates oxygen activation, forming O_2^- species.[52] This is in accordance with the DFT calculation presented above and also demonstrates that the O_2 is more easily absorbed on the surface of Au−Ag, resulting in the enhancement of the rate-relevant step.

3.2. Effect of the Au/Ag Ratio and Plausible Catalyst Structure−Activity Relationship. To further understand the unique synergy effects of Au−Ag nanoparticles, bimetallic Au−Ag/TS-1-B catalysts with different Au/Ag molar ratios were also prepared and tested. Au loadings are kept almost the same and low in order to make sure the conversions are similar and less than 5%. It can be seen in Figure 1d that the stable PO formation rate first increases with the decrease in the Au/Ag molar ratio, followed by a decrease in activity. The maximum value (i.e., 174 g_{PO} h^{-1} g_{Au}^{-1}) is achieved at a Au/Ag molar ratio of 10/1. The physical mixture of Au/TS-1-B and Ag/TS-1-B catalysts shows a worse performance than those of the Au_{10}−Ag_1/TS-1-B catalyst. Moreover, HAADF-STEM and HRTEM measurements of three selected catalysts (i.e., Au_{20}−Ag_1/TS-1-B, Au_{10}−Ag_1/TS-1-B, and Au_2−Ag_1/TS-1-B) are shown in Figure 2. Their average metal particle sizes are quite similar. These results indicate that the difference in the metal particle size could not be the dominant reason for the difference in the PO formation rate of different Au−Ag/TS-1-B catalysts.

In principle, with the decrease in the Au/Ag molar ratio, the nature of bimetallic Au−Ag nanoparticles should be different, which is most likely responsible for the different PO formation rates of the bimetallic catalysts. Because of the extremely low loadings of Au and Ag and the small particle size, EDS and TPR are unable to give reliable results.[39] UV−vis DRS was then employed to study the nature of bimetallic nanoparticles as a function of Au/Ag molar ratio, and the results are shown in Figure 5. Clearly, when the Au/Ag molar ratios are 30/1, 20/1, and 10/1, the catalysts exhibit only one absorption band. In comparison to the adsorption band of the Au/TS-1-B catalyst, the adsorption bands of Au_{30}−Ag_1/TS-1-B, Au_{20}−Ag_1/TS-1-B, and Au_{10}−Ag_1/TS-1-B catalysts are blue-shifted to 521, 512, and 507 nm, respectively. As described above, these bimetallic catalysts have similar metal particle sizes. Therefore, the blue-shifted adsorption bands could be due to different alloy compositions of bimetallic Au−Ag nanoparticles that originated from different Au/Ag molar ratios.[25,53−57] This could provide an interpretation for the increased PO formation rate of bimetallic Au−Ag/TS-1-B catalysts with the decrease in the Au/Ag molar ratio from 30/1 to 10/1. Moreover, it can also be seen in Figure 5 that further decreasing the Au/Ag molar ratio from 6/1 to 2/1 leads to the presence of a Ag peak at 410 nm, which might result from the segregation of Ag on a catalyst.[58] On one hand, the Ag sites may lead to the breaking of the allylic C−H bond in propene by the highly active O_2^- and complete oxidation to CO_2.[59] On the other hand, the segregated Ag particles might exist on the Au surfaces, covering

Table 1. Comparison of the Stable Catalytic Performances of Catalysts

catalyst	reaction temperature (K)	GHSV ($cm^3\ h^{-1}\ g_{cat}^{-1}$)	PO formation rate ($g_{PO}\ h^{-1}\ g_{Au}^{-1}$)	PO selectivity (%)	ref
Au_{10}–Ag_1/TS-1-B	473	14000	174	84	this work
Au_{10}–Ag_1/TS-1-B	493	14000	233	73	this work
Au/TS-1	573	7000	32	72	60
Au/TS-1	473	14000	110	–	61
Au/Ti-SiO_2	473	10000	110	92	46
Au/TS-1-Na1	473	8000	119	85	62

the number of Au active sites. These could explain the lower PO formation rates of the bimetallic catalysts with a much lower Au/Ag molar ratio. This is demonstrated by the decrease in PO selectivity from 85 to 75% with the decrease in the Au/Ag molar ratio from 1/0 to 2/1.

The catalytic activity of the optimum Au_{10}–Ag_1/TS-1-B catalyst is tested at higher reaction temperatures. It is found that the PO formation rate of the Au–Ag/TS-1-B catalyst at 493 K shows a higher activity of 233 $g_{PO}\ h^{-1}\ g_{Au}^{-1}$, much higher than that of the Au/TS-1-B catalyst. Table 1 gives a comparison of the stable PO formation rates between the optimal Au_{10}–Ag_1/TS-1-B catalyst and other reported catalysts.[60−62] It should be noted that the reported Cs–Au/TS-1 catalyst[20] shows a quite fascinating PO formation rate of ~300 $g_{PO}\ h^{-1}\ kg_{cat}^{-1}$ but not included herein because using traditional TS-1 as a support may lead to micropore blocking deactivation.[24] Obviously, Au/TS-1-B with blocked micropores of TS-1 shows a high stable PO formation rate because the use of the TS-1-B support suppresses the deactivation of micropore blocking and avoids the invalidation of the Au particles inside TS-1 micropores, maintaining a high stable PO formation rate. Importantly, the Au_{10}–Ag_1/TS-1-B catalyst shows a much higher stable PO formation rate. The insights revealed herein shed new light on the design of efficient catalysts for direct propene epoxidation that suffer from severe deactivation and low activity. In addition, the methodology using DFT and multiple types of characterization (e.g., HAADF-STEM, UV–vis, and XPS) could be extended to elucidate the nature of promoters for other bimetallic catalysts.

4. CONCLUSIONS

In summary, we envision a novel strategy for simultaneously improving the catalytic activity and stability by synthesizing the Au–Ag/TS-1-B catalyst, and the structural–performance relationship is systematically studied. By DFT, multiple types of characterization, and experiments, it is found that the addition of Ag effectively enhances the dispersion of Au nanoparticles (~2.7 nm) on the external surfaces of TS-1-B. The resultant Au–Ag bimetallic nanoparticles, most likely in the form of an alloy, lead to a surge in the PO formation rate and H_2 efficiency to 44%. In addition, the Au–Ag catalyst shows better oxygen adsorption ability and facilitates electron transfer from Au to O_2. Furthermore, there is a volcano-shaped relationship between the Au/Ag ratio and catalytic performance. The PO formation rate increases with a decrease in the Au/Ag ratio to a maximum value of 174–233 $g_{PO}\ h^{-1}\ g_{Au}^{-1}$ at a Au/Ag molar ratio of 10/1 followed by a decline in activity. The decreasing trend of the PO formation rate possibly results from the existence of more Ag sites, leading to the coverage of Au active sites and the occurrence of side reactions. These results demonstrate that addition of Ag plays a crucial role in the design and optimization of Au-based/TS-1-B catalysts with stable reactivity for propene epoxidation with H_2 and O_2. It is expected that this work is significantly important to the design of other bimetallic catalysts for propene epoxidation.

■ ASSOCIATED CONTENT

Supporting Information

The Supporting Information is available free of charge on the ACS Publications website at DOI: 10.1021/acscatal.8b01324.

Characterization data and DFT results (PDF)

■ AUTHOR INFORMATION

Corresponding Authors

*E-mail: xiangfeng@upc.edu.cn.

*E-mail: xgzhou@ecust.edu.cn.

ORCID

Xiang Feng: 0000-0001-7299-5690

Xuezhi Duan: 0000-0002-5843-5950

Chaohe Yang: 0000-0001-6995-9170

Notes

The authors declare no competing financial interest.

■ ACKNOWLEDGMENTS

This work was supported by the National Science Foundation of China (Grant 21606254), the Key Research and Development Plan of Shandong Province (2017GSF17126), the Natural Science Foundation of Shandong Province (ZR2016BB16), the Independent Innovation Foundation of Qingdao (17-1-1-18-jch), and Fundamental Research Funds for the Central Universities (18CX02014A).

■ REFERENCES

(1) Hayashi, T.; Tanaka, K.; Haruta, M. Selective vapor-phase epoxidation of propylene over Au/TiO_2 catalysts in the presence of oxygen and hydrogen. *J. Catal.* **1998**, *178*, 566–575.

(2) Yap, N.; Andres, R. P.; Delgass, W. N. Reactivity and stability of Au in and on TS-1 for epoxidation of propylene with H_2 and O_2. *J. Catal.* **2004**, *226*, 156–170.

(3) Song, A. N.; Feng, X.; Sheng, N.; Lin, D.; Li, Y. C.; Liu, Y. B.; Chen, X. B.; Zhou, X. G.; Chen, D.; Yang, C. H. Propene epoxidation with H_2 and O_2 on Au/TS-1 catalyst: Cost-effective synthesis of small-sized mesoporous TS-1 and its unique performance. *Catal. Today*, **2018**, .

(4) Bravo-Suárez, J. J.; Bando, K. K.; Lu, J.; Haruta, M.; Fujitani, T.; Oyama, S. T. Transient technique for identification of true reaction intermediates: Hydroperoxide species in propylene epoxidation on gold/titanosilicate catalysts by X-ray absorption fine structure spectroscopy. *J. Phys. Chem. C* **2008**, *112*, 1115–1123.

(5) Lu, J.; Zhang, X.; Bravo-Suárez, J. J.; Bando, K. K.; Fujitani, T.; Oyama, S. T. Direct propylene epoxidation over barium-promoted Au/Ti-TUD catalysts with H_2 and O_2: Effect of Au Particle Size. *J. Catal.* **2007**, *250*, 350–359.

(6) Chowdhury, B.; Bravo-Suárez, J. J.; Daté, M.; Tsubota, S.; Haruta, M. Trimethylamine as a gas-phase promoter: Highly efficient epoxidation of propylene over supported gold catalysts. *Angew. Chem., Int. Ed.* **2006**, *45*, 412–415.

(7) Haruta, M. Catalysis of gold nanoparticles deposited on metal oxides. *CATTECH* **2002**, *6*, 102−115.
(8) Chen, J.; Halin, S. J.; Pidko, E. A.; Verhoeven, M.; Ferrandez, D. M. P.; Hensen, E. J.; Schouten, J. C.; Nijhuis, T. A. Enhancement of catalyst performance in the direct propene epoxidation: A study into gold-titanium synergy. *ChemCatChem* **2013**, *5*, 467−478.
(9) Feng, X.; Chen, D.; Zhou, X. G. Thermal stability of TPA template and size-dependent selectivity of uncalcined TS-1 supported Au catalyst for propene epoxidation with H_2 and O_2. *RSC Adv.* **2016**, *6*, 44050−44056.
(10) Qi, C.; Akita, T.; Okumura, M.; Kuraoka, K.; Haruta, M. Effect of surface chemical Properties and texture of mesoporous titanosilicates on direct vapor-phase epoxidation of propylene over Au catalysts at high reaction temperature. *Appl. Catal., A* **2003**, *253*, 75−89.
(11) Liu, Y.; Zhang, X.; Suo, J. Gold supported on nitrogen-incorporated TS-1 for gas-phase epoxidation of propylene. *Chin. J. Catal.* **2013**, *34*, 336−340.
(12) Lu, X.; Zhao, G. F.; Lu, Y. Propylene epoxidation with O_2 and H_2: a high-performance Au/TS-1 catalyst prepared via deposition-precipitation using urea. *Catal. Sci. Technol.* **2013**, *3*, 2906−2909.
(13) Feng, X.; Duan, X.; Cheng, H.; Qian, G.; Chen, D.; Yuan, W.; Zhou, X. Au/TS-1 Catalyst prepared by deposition-precipitation method for propene epoxidation with H_2/O_2: Insights into the effects of slurry aging time and Si/Ti molar ratio. *J. Catal.* **2015**, *325*, 128−135.
(14) Zanella, R.; Giorgio, S.; Henry, C. R.; Louis, C. Alternative methods for the preparation of gold nanoparticles supported on TiO_2. *J. Phys. Chem. B* **2002**, *106*, 7634−7642.
(15) Feng, X.; Duan, X.; Qian, G.; Zhou, X.; Chen, D.; Yuan, W. Insights into size-dependent activity and active sites of Au nanoparticles supported on TS-1 for propene epoxidation with H_2 and O_2. *J. Catal.* **2014**, *317*, 99−104.
(16) Feng, X.; Liu, Y.; Li, Y.; Yang, C.; Zhang, Z.; Duan, X.; Zhou, X.; Chen, D. Au/TS-1 catalyst for propene epoxidation with H_2/O_2: A novel strategy to enhance stability by tuning charging sequence. *AIChE J.* **2016**, *62*, 3963−3972.
(17) Feng, X.; Sheng, N.; Liu, Y.; Chen, X.; Chen, D.; Yang, C.; Zhou, X. Simultaneously enhanced stability and selectivity for propene epoxidation with H_2 and O_2 on Au catalysts supported on nano-crystalline mesoporous TS-1. *ACS Catal.* **2017**, *7*, 2668−2675.
(18) Shekhar, M.; Wang, J.; Lee, W. S.; Williams, W. D.; Kim, S. M.; Stach, E. A.; Miller, J. T.; Delgass, W. N.; Ribeiro, F. H. Size and support effects for the water-gas shift catalysis over gold nanoparticles supported on model Al_2O_3 and TiO_2. *J. Am. Chem. Soc.* **2012**, *134*, 4700−4708.
(19) Feng, X.; Duan, X.; Yang, J.; Qian, G.; Zhou, X.; Chen, D.; Yuan, W. Au/uncalcined TS-1 catalysts for direct propene epoxidation with H_2 and O_2: Effects of Si/Ti molar ratio and Au loading. *Chem. Eng. J.* **2015**, *278*, 234−239.
(20) Lee, W. S.; Cem Akatay, M.; Stach, E. A.; Ribeiro, F. H.; Delgass, W. N. Enhanced reaction rate for gas-phase epoxidation of propylene using H_2 and O_2 by Cs promotion of Au/TS-1. *J. Catal.* **2013**, *308*, 98−113.
(21) Lu, J.; Zhang, X.; Bravo-Suárez, J. J.; Fujitani, T.; Oyama, S. T. Effect of composition and promoters in Au/TS-1 catalysts for direct propylene epoxidation using H_2 and O_2. *Catal. Today* **2009**, *147*, 186−195.
(22) Li, Z.; Zhang, J.; Wang, D.; Ma, W.; Zhong, Q. Confirmation of gold active sites on titanium-silicalite-1-supported nano-gold catalysts for gas-phase epoxidation of propylene. *J. Phys. Chem. C* **2017**, *121*, 25215−25222.
(23) Lu, J.; Zhang, X.; Bravo-Suárez, J. J.; Fujitani, T.; Oyama, S. T. Effect of composition and promoters in Au/TS-1 catalysts for direct propylene epoxidation using H_2 and O_2. *Catal. Today* **2009**, *147*, 186−195.
(24) Lee, W. S.; Cem Akatay, M.; Stach, E. A.; Ribeiro, F. H.; Delgass, W. N. Enhanced reaction rate for gas-phase epoxidation of propylene using H_2 and O_2 by Cs promotion of Au/TS-1. *J. Catal.* **2013**, *308*, 98−113.
(25) Feng, X.; Duan, X.; Qian, G.; Zhou, X.; Chen, D.; Yuan, W. Au nanoparticles deposited on the external surfaces of TS-1: Enhanced stability and activity for direct propylene epoxidation with H_2 and O_2. *Appl. Catal., B* **2014**, *150−151*, 396−401.
(26) Sandoval, A.; Aguilar, A.; Louis, C.; Traverse, A.; Zanella, R. Bimetallic Au-Ag/TiO_2 catalyst prepared by deposition-precipitation: High activity and stability in CO oxidation and stability in CO oxidation. *J. Catal.* **2011**, *281*, 40−49.
(27) Henkelman, G.; Arnaldsson, A.; Jónsson, H. A fast and robust algorithm for Bader decomposition of charge density. *Comput. Mater. Sci.* **2006**, *36*, 354−360.
(28) Sanville, E.; Kenny, S. D.; Smith, R.; Henkelman, G. Improved grid-based algorithm for Bader charge allocation. *J. Comput. Chem.* **2007**, *28*, 899−908.
(29) Yamazoe, S.; Koyasu, K.; Tsukuda, T. Nonscalable oxidation catalysis of gold clusters. *Acc. Chem. Res.* **2014**, *47*, 816−824.
(30) Bravo-Suarez, J. J.; Bando, K. K.; Lu, J.; Haruta, M.; Fujitani, T.; Oyama, T. Transient technique for identification of true reaction intermediates: Hydroperoxide species in propylene epoxidation on gold/titanosilicate catalysts by X-ray absorption fine structure spectroscopy. *J. Phys. Chem. C* **2008**, *112*, 1115−1123.
(31) Hugon, A.; El Kolli, N.; Louis, C. Advances in the preparation of supported gold catalysts: Mechanism of deposition, simplification of the procedures and relevance of the elimination of chlorine. *J. Catal.* **2010**, *274*, 239−250.
(32) Sandoval, A.; Aguilar, A.; Louis, C.; Traverse, A.; Zanella, R. Bimetallic Au-Ag/TiO_2 catalyst prepared by deposition-precipitation: High activity and stability in CO oxidation. *J. Catal.* **2011**, *281*, 40−49.
(33) Sandoval, A.; Delannoy, L.; Méthivier, C.; Louis, C.; Zanella, R. Synergetic effect in bimetallic Au-Ag/TiO_2 catalysts for CO oxidation: New insights from in situ characterization. *Appl. Catal., A* **2015**, *504*, 287−294.
(34) Wells, D. H.; Delgass, W. N.; Thomson, K. T. Formation of hydrogen peroxide from H_2 and O_2 over a neutral gold trimer: a DFT study. *J. Catal.* **2004**, *225*, 69−77.
(35) Boronat, M.; Corma, A. Oxygen activation on gold nanoparticles: Separating the influence of particle size, particle shape and support interaction. *Dalton Trans.* **2010**, *39*, 8538−8546.
(36) Taylor, B.; Lauterbach, J.; Delgass, W. N. Gas-phase epoxidation of propylene over small gold ensembles on TS-1. *Appl. Catal., A* **2005**, *291*, 188−198.
(37) Barton, D. G.; Podkolzin, S. G. Kinetic study of a direct water synthesis over silica-supported gold nanoparticles. *J. Phys. Chem. B* **2005**, *109*, 2262−2274.
(38) Du, M.; Zhan, G.; Yang, X.; Wang, H.; Lin, W.; Zhou, Y.; Zhu, J.; Lin, L.; Huang, J.; Sun, D.; Jia, L.; Li, Q. Ionic liquid-enhanced immobilization of biosynthesized Au nanoparticles on TS-1 toward efficient catalysts for propylene epoxidation. *J. Catal.* **2011**, *283*, 192−201.
(39) Hanawalt, J. D.; Rinn, H. W.; Frevel, L. K. Chemical Analysis by X-Ray Diffraction. *Ind. Eng. Chem., Anal. Ed.* **1938**, *10*, 457−512.
(40) Wang, A. Q.; Liu, J.-H.; Lin, S. D.; Lin, T. S.; Mou, C. Y. A novel efficient Au−Ag alloy catalyst system: preparation, activity, and characterization. *J. Catal.* **2005**, *233*, 186−197.
(41) Ruban, A.; Skriver, H. L.; Nørskov, J. K. Surface segregation energies in transition-metal alloys. *Phys. Rev. B: Condens. Matter Mater. Phys.* **1999**, *59*, 15990−16000.
(42) Li, Y.; Zhang, B. P.; Zhao, J. X. Enhanced photocatalytic performance of Au-Ag alloy modified ZnO nanocomposite films. *J. Alloys Compd.* **2014**, *586*, 663−668.
(43) Tahir, M.; Tahir, B.; Amin, N. A. S. Synergistic effect in plasmonic Au/Ag alloy NPs co-coated TiO_2 NWs toward visible-light enhanced CO_2 photoreduction to fuels. *Appl. Catal., B* **2017**, *204*, 548−560.
(44) Crespo, J.; Falqui, A.; Garcia-Barrasa, J.; Lopez-de-Luzuriaga, J. M.; Monge, M.; Olmos, M. E.; Rodriguez-Castillo, M.; Sestu, M.;

Soulantica, K. Synthesis and plasmonic properties of monodisperse Au-Ag alloy nanoparticles of different compositions from a single-source organometallic precursor. *J. Mater. Chem. C* **2014**, *2*, 2975−2984.
(45) Han, C.; Yang, X.; Gao, G.; Wang, J.; Lu, H.; Liu, J.; Tong, M.; Liang, X. Selective oxidation of methanol to methyl formate on catalysts of Au-Ag alloy nanoparticles supported on titania under UV irradiation. *Green Chem.* **2014**, *16*, 3603−3615.
(46) Kanungo, S.; Keshri, K. S.; Van Hoof, A. J. F; Neira d'Angelo, M. F.; Schouten, J. C.; Nijhuis, T. A.; Hensen, E. J. M; Chowdhury, B. Silylation enhances the performance of Au/Ti-SiO_2 catalysts in direct epoxidation of propene using H_2 and O_2. *J. Catal.* **2016**, *344*, 434−444.
(47) Fujita, T.; Guan, P.; McKenna, K.; Lang, X.; Hirata, A.; Zhang, L.; Tokunaga, T.; Arai, S.; Yamamoto, Y.; Tanaka, N.; Ishikawa, Y.; Asao, N.; Yamamoto, Y.; Erlebacher, J.; Chen, M. Atomic origins of the high catalytic activity of nanoporous gold. *Nat. Mater.* **2012**, *11*, 775−780.
(48) Slater, T. J. A.; Macedo, A.; Schroeder, S. L. M.; Burke, M. G.; O'Brien, P.; Camargo, P. H. C.; Haigh, S. J. Correlating Catalytic Activity of Ag-Au Nanoparticles with 3D Compositional Variations. *Nano Lett.* **2014**, *14*, 1921−1926.
(49) Li, Q.; Zhang, Y.; Chen, G.; Fan, J.; Lan, H.; Yang, Y. Ultra-low-gold loading Au/CeO_2 catalysts for ambient temperature CO oxidation: Effect of preparation conditions on surface composition and activity. *J. Catal.* **2010**, *273*, 167−176.
(50) Liu, H.; Lu, G.; Hu, H. Synthesis, characterization and catalytic performance of titanium silicalite-1 prepared in the presence of nonionic surfactants. *Mater. Chem. Phys.* **2006**, *100*, 162−167.
(51) Wei, Y.; Zhao, Z.; Liu, J.; Liu, S.; Xu, C.; Duan, A.; Jiang, G. Multifunctional catalysts of three-dimensionally ordered macroporous oxide-supported Au@Pt core-shell nanoparticles with high catalytic activity and stability for soot oxidation. *J. Catal.* **2014**, *317*, 62−74.
(52) Yen, C. W.; Lin, M.-L.; Wang, A.; Chen, S. A.; Chen, J. M.; Mou, C. Y. CO Oxidation Catalyzed by Au-Ag Bimetallic Nanoparticles Supported in Mesoporous Silica. *J. Phys. Chem. C* **2009**, *113*, 17831−17839.
(53) Sandoval, A.; Delannoy, L.; Méthivier, C.; Louis, C.; Zanella, R. Synergetic effect in bimetallic Au-Ag TiO_2 catalysts for CO oxidation: New insights from in situ characterization. *Appl. Catal., A* **2015**, *504*, 287−294.
(54) Liu, J. H.; Wang, A. Q.; Chi, Y. S.; Lin, H. P.; Mou, C. Y. Synergistic effect in an Au-Ag alloy nanocatalyst: CO Oxidation. *J. Phys. Chem. B* **2005**, *109*, 40−43.
(55) Wang, A. Q.; Liu, J. H.; Lin, S. D.; Lin, T. S.; Mou, C. Y. A Novel Efficient Au-Ag alloy catalyst system: Preparation, activity, and characterization. *J. Catal.* **2005**, *233*, 186−197.
(56) Qu, Z.; Ke, G.; Wang, Y.; Liu, M.; Jiang, T.; Gao, J. Investigation of factors influencing the catalytic performance of CO oxidation over Au-Ag/SBA-15 catalyst. *Appl. Surf. Sci.* **2013**, *277*, 293−301.
(57) Zemichael, F. W.; Al-Musa, A.; Cumming, I. W.; Hellgardt, K. Propene Partial Oxidation over Au-Ag alloy and Ag catalysts using electrochemical oxygen. *Solid State Ionics* **2008**, *179*, 1401−1404.
(58) Deng, L.; Hu, W.; Deng, H.; Xiao, S.; Tang, J. Au-Ag bimetallic nanoparticles: Surface segregation and atomic-scale structure. *J. Phys. Chem. C* **2011**, *115*, 11355−11363.
(59) Huang, J.; Haruta, M. Gas-phase propene epoxidation over coinage metal catalysts. *Res. Chem. Intermed.* **2012**, *38*, 1−24.
(60) Du, M.; Zhan, G.; Yang, X.; Wang, H.; Lin, W.; Zhou, Y.; Zhu, J.; Lin, L.; Huang, J.; Sun, D.; Jia, L.; Li, Q. Ionic liquid-enhanced immobilization of biosynthesized Au nanoparticles on TS-1 toward efficient catalysts for propylene epoxidation. *J. Catal.* **2011**, *283*, 192−201.
(61) Lee, W.-S.; Cem Akatay, M.; Stach, E. A.; Ribeiro, F. H.; Delgass, W. N. Reproducible preparation of Au/TS-1 with high reaction rate for gas phase epoxidation of propylene. *J. Catal.* **2012**, *287*, 178−189.
(62) Huang, J.; Takei, T.; Akita, T.; Ohashi, H.; Haruta, M. Gold clusters supported on alkaline treated TS-1 for highly efficient propene epoxidation with O_2 and H_2. *Appl. Catal., B* **2010**, *95*, 430−438.